Global and Planetary Change 178 (2019) 139–152

Contents lists available at ScienceDirect

Global and Planetary Change

journal homepage: www.elsevier.com/locate/gloplacha

Arctic vegetation, temperature, and hydrology during Early Eocene transient global warming events

Debra A. Willard[a,*], Timme H. Donders[b], Tammo Reichgelt[c], David R. Greenwood[d], Francesca Sangiorgi[e], Francien Peterse[e], Klaas G.J. Nierop[e], Joost Frieling[e], Stefan Schouten[e,f], Appy Sluijs[e]

[a] US Geological Survey, 926A National Center, 12201 Sunrise Valley Drive, Reston, VA 20192, United States of America
[b] Department of Physical Geography, Utrecht University, Princetonlaan 8a, 3584 CB Utrecht, The Netherlands
[c] Lamont-Doherty Earth Observatory, Columbia University, 61 Route 9W, P.O. Box 1000, Palisades, NY 10964, United States of America
[d] Department of Biology, Brandon University, J.R. Brodie Science Centre, 270 18th Street, Brandon, MB, R7A 6A9, Canada
[e] Department of Earth Sciences, Utrecht University, Princetonlaan 8a, 3584 CB Utrecht, The Netherlands
[f] NIOZ Royal Netherlands Institute for Sea Research, 1790AB Den Burg, Texel, The Netherlands

ARTICLE INFO

Keywords:
Palynology
Palynofacies
brGDGTs
Bioclimatic reconstructions
Paleocene-Eocene Thermal Maximum
ETM2
Arctic
Paleoclimate

ABSTRACT

Early Eocene global climate was warmer than much of the Cenozoic and was punctuated by a series of transient warming events or 'hyperthermals' associated with carbon isotope excursions when temperature increased by 4–8 °C. The Paleocene-Eocene Thermal Maximum (PETM, ~55 Ma) and Eocene Thermal Maximum 2 (ETM2, 53.5 Ma) hyperthermals were of short duration (< 200 kyr) and dramatically restructured terrestrial vegetation and mammalian faunas at mid-latitudes. Data on the character and magnitude of change in terrestrial vegetation and climate during and after the PETM and ETM2 at high northern latitudes, however, are limited to a small number of stratigraphically restricted records. The Arctic Coring Expedition (ACEX) marine sediment core from the Lomonosov Ridge in the Arctic Basin provides a stratigraphically expanded early Eocene record of Arctic terrestrial vegetation and climates. Using pollen/spore assemblages, palynofacies data, bioclimatic analyses (Nearest Living Relative, or NLR), and lipid biomarker paleothermometry, we present evidence for expansion of mesothermal (Mean Annual Temperatures 13–20 °C) forests to the Arctic during the PETM and ETM2. Our data indicate that PETM mean annual temperatures were ~2° to 3.5 °C warmer than those of the Late Paleocene. Mean winter temperatures in the PETM reached ≥5 °C (~2 °C warmer than the late Paleocene), based on pollen-based bioclimatic reconstructions and the presence of palm and Bombacoideae pollen. Increased runoff of water and nutrients to the ocean during both hyperthermals resulted in greater salinity stratification and hypoxia/anoxia, based on marked increases in concentration of massive Amorphous Organic Matter (AOM) and dominance of low-salinity dinocysts. During the PETM recovery, taxodioid Cupressaceae-dominated swamp forests were important elements of the landscape, representing intermediate climate conditions between the early Eocene hyperthermals and background conditions of the late Paleocene.

1. Introduction

The Paleocene-Eocene Thermal Maximum (PETM; ~56 million years ago; Ma) and Eocene Thermal Maximum 2 (ETM2; ~54 Ma) were global warming events of < 200 kyrs in duration (Dunkley Jones et al., 2013; Lourens et al., 2005; Zachos, 2005). They were associated with massive injections of ^{13}C-depleted carbon into the ocean-atmosphere system, evidenced by massive deep-sea carbonate dissolution and a 2–5‰ negative carbon isotope excursion (CIE) in sediments (Sluijs and Dickens, 2012). These 'hyperthermals' provide valuable, albeit imperfect, analogues for models of future climate change, offering opportunities to document the behavior of the hydrological cycle during past periods of global warming (Pierrehumbert, 2002). Although warming during the hyperthermals was widespread and especially pronounced in polar regions (Dunkley Jones et al., 2013; Sluijs et al., 2009, 2006; Stap et al., 2010a), and some Arctic precipitation

* Corresponding author.
E-mail addresses: dwillard@usgs.gov (D.A. Willard), t.h.donders@uu.nl (T.H. Donders), tammor@ldeo.columbia.edu (T. Reichgelt), greenwoodd@brandonu.ca (D.R. Greenwood), F.sangiorgi@uu.nl (F. Sangiorgi), f.peterse@uu.nl (F. Peterse), k.g.j.nierop@uu.nl (K.G.J. Nierop), J.frieling1@uu.nl (J. Frieling), stefan.schouten@nioz.nl (S. Schouten), A.sluijs@uu.nl (A. Sluijs).

https://doi.org/10.1016/j.gloplacha.2019.04.012
Received 25 February 2019; Received in revised form 11 April 2019; Accepted 12 April 2019
Available online 24 April 2019

reconstructions are available (Eldrett et al., 2014; Pagani et al., 2006), reconstructions of seasonality and hydrology of polar climates are limited. Many records have imprecise stratigraphies relative to the PETM and ETM2 (e.g. Greenwood et al., 2010; West et al., 2015), and well-dated terrestrial paleoclimate reconstructions of Eocene hyperthermals are scarce.

Carbon injection into the atmosphere and associated global warming are hypothesized to invigorate the global hydrological cycle and at least regionally amplify seasonal contrasts (Masson-Delmotte, 2013). These responses are hypothesized for the PETM and ETM2, which were associated with pronounced increases of atmospheric CO_2 concentrations (Panchuk et al., 2008; Zeebe et al., 2009), and ~5 °C and ~3 °C of global average surface warming, respectively (Dunkley Jones et al., 2013; Stap et al., 2010a). To test this hypothesis, we reconstructed terrestrial vegetation and climates from marginal marine upper Paleocene and lower Eocene strata recovered from Lomonosov Ridge, Arctic Ocean, during Integrated Ocean Drilling Program (IODP) Expedition 302, termed the Arctic Coring Expedition (ACEX) (Moran et al., 2006). Reconstructions herein are based on bioclimatic analysis of pollen and spore assemblages, analysis of branched glycerol dialkyl glycerol tetraether (brGDGT) bacterial membrane lipids, and palynofacies analysis. Sediments in the ACEX cores were deposited close to shore at a paleolatitude of ~85°N and consist of organic-rich mudstones that lack biogenic calcite. The PETM and ETM2, which were identified based on biostratigraphy and isotope stratigraphy, consist of laminated sediments (Pagani et al., 2006; Sluijs et al., 2009). Pollen, spores, phytodebris, and biomarkers were most likely derived from exposed parts of the Lomonosov Ridge or the Asian continent, which were close to the study site at the time of deposition (Martinez et al., 2009). Although taphonomic factors such as differential transport of pollen by wind and water and reworking of sediment complicate interpretation of pollen assemblages from marine units, the composition of pollen assemblages in marine surface samples on continental margins generally corresponds to modern vegetation assemblages onshore (Mudie and McCarthy, 1994). Because distribution of the source vegetation is controlled by a combination of climatic and edaphic factors, pollen-based reconstructions of vegetational change provide insights into patterns of polar seasonal variability before, during, and after the hyperthermal events. Here we quantify seasonality of temperature and precipitation across the PETM and ETM2 based on pollen, spore, and palynofacies assemblages recovered in sediment cores from Lomonosov Ridge, central Arctic Ocean.

2. Materials and methods

2.1. Locality and stratigraphy

The Integrated Ocean Drilling Program (IODP) Site 302 is located on the Lomonosov Ridge in the central Arctic Ocean (87° 52.00′ N; 136° 10.64′ E, 1288 m water depth) (Fig. 1), where > 400 m of sediment core was recovered. Upper Paleocene through Lower Eocene sediments between 391 and 367 m composite depth below sea floor (mcd) consist of organic rich claystones (Backman et al., 2006; Moran et al., 2006) that yielded abundant palynomorph assemblages, including dinocysts, pollen and spores of terrestrial plants, phytodebris, and amorphous organic matter. The Paleocene-Eocene Thermal Maximum (PETM) was identified between ~387 and 378.5 mcd by the presence of the dinocyst *Apectodinium augustum* (Sluijs et al., 2006). Drilling disturbance in the upper 50 cm of Core 32× and poor core recovery from the overlying Core 31× makes identification of the lower boundary problematic, but an ~6‰ decrease in stable isotopes of bulk organic carbon ($\delta^{13}C_{TOC}$) between the top of Core 32× and the base of Core 31× indicates the onset of the PETM by at least 386.1 mcd (Sluijs et al., 2006) (Fig. 2a). The body of the PETM, corresponding to the peak CIE, spans the interval from 386.1–383.23 mcd, with the recovery zone extending from 383.03 mcd to the upper limit of *A. augustum* at 378.5 mcd.

The ETM2 hyperthermal event was identified between 368.94 and ~368.2 mcd, based on a ~3.5‰ negative carbon isotope excursion (CIE) (Sluijs et al., 2009) (Fig. 2). A laminated, glauconite-rich unit (371–368.94 mcd) underlying the ETM2 is characterized by an ~2‰ negative CIE, relative to background levels. This unit, which we refer to as the pre-ETM2 interval, is characterized by distinctive palynological assemblages and may correspond to earliest phases of the ETM2 observed in the southern ocean (Lourens et al., 2005; Stap et al., 2010a,b).

2.2. Pollen and palynofacies analyses

The Paleocene – Lower Eocene section of Site 302-4A was sampled at 0.1–0.3 m intervals from 367 to 391 mcd for analysis of organic-walled microfossils. Sediments were oven dried at 60 °C and weighed. Tablets with known numbers of *Lycopodium* spores were added to approximately 2 g dry sediment before being treated with hydrochloric and hydrofluoric acids to remove carbonates and silicates, respectively. Residues were sieved with 15 μm mesh and mounted on microscope slides in glycerin jelly. Pollen analyses relied on counts of at least 300 grains (or a minimum of 100 in samples with sparse palynomorphs). Concentration of palynomorphs (grains/g dry sediment) were calculated based on relative abundance of fossil palynomorphs and *Lycopodium* spores, following procedures outlined in (Stockmarr, 1971). The *Lycopodium* marker grains were distinguished from the fossil grain *Lycpodiumsporites* by the three-dimensional preservation of the marker grains and typically better-preserved ornamentation. Detrended Correspondence Analysis (DCA) was used to identify the main factors among the pollen data; only taxa that represented > 2% of assemblages in at least one sample were included in the analysis, using the software program Past 3.20. In addition, Excel was used to plot the stratigraphic distribution of pollen and spore taxa as first and last appearances.

Palynofacies analyses used counts of at least 500 palynomorphs to provide a quantitative analysis of total particulate organic matter (all acid-resistant dispersed sedimentary organic matter, such as pollen, spores, phytoclasts, algae, foraminiferal linings, dinocysts, and amorphous organic matter [AOM]) (Batten, 1996). Palynomorphs were classified as pollen and spores (Fig. 3d,e), dinoflagellate cysts (dinocysts) (Fig. 3b,c) (Sluijs et al., 2009, 2006), angular opaque material (Fig. 3c,d), granular AOM (Fig. 3d,f,g,h), fluorescent AOM (Fig. 3g,h), and massive AOM (Fig. 3a,b,e,g,h). Angular opaque materials consist of phytoclasts with varying degrees of structural preservation (Batten, 1996). Amorphous organic matter includes unstructured organic particles that have been degraded by physical or microbial means (Batten, 1996; Ercegovac and Kostić, 2006; Wood and Gorin, 1998).

2.3. Bioclimatic analysis

Bioclimatic Analysis is a paleoclimatic proxy that employs the climatic range of modern living relatives of plants found together in a fossil assemblage and statistically constrains the most likely climatic co-occurrence envelope (Greenwood et al., 2017, 2005, 2003; Reichgelt et al., 2018; Thompson et al., 2012). For this study, we used living relative global distributions of fossil taxa and constrained the bioclimatic range of these taxa for mean annual temperature (MAT), summer (Jun-Jul-Aug) and winter (Dec-Jan-Feb) average temperature (ST and WT), mean annual precipitation (MAP) and summer and winter precipitation (SP and WP) by cross-plotting plant modern distributions from the Global Biodiversity Information Facility (GBIF.org 2018) with gridded climatic maps using the 'dismo' package in R (Hijmans et al. 2005). Prior to calculating climatic range of modern plants, the geodetic data was filtered for:

1. Plants with doubtful taxonomic assignments.
2. Exotic, invasive and garden plants.
3. Redundant occurrences.

Fig. 1. Location of IODP Site 302-4A, Lomonosov Ridge, central Arctic Ocean (red circle) and other northern hemisphere sites with late Paleocene to early Eocene records (yellow circles): North Slope, Sagwon Alaska (Daly et al., 2011); Mackenzie Delta (McNeil and Parsons, 2013); Ellesmere Island (Greenwood et al., 2010; Greenwood and Basinger, 1994; West et al., 2015); Bighorn Basin (Wing, 2005); Spitsbergen (Harding et al., 2011); North Sea (Eldrett et al., 2014); and New Siberia Islands (Suan et al., 2017). (For interpretation of the references to colour in this figure legend, the reader is referred to the web version of this article.)

For each taxon, probability density functions of MAT, ST, WT, MAP, SP and WP were calculated using the mean and standard deviation of their climatic distribution (Table 1).

Climatic envelopes were constrained by calculating the probability of the climatic envelopes of taxa overlapping (Greenwood et al. 2017; Hyland et al. 2018; Reichgelt et al. 2018). The rationale behind this method is that optimal climatic conditions of taxa are reflected in their modern range and that these combined probability density functions can therefore be used to calculate the most likely climatic situation in which these taxa can co-occur (Harbert and Nixon 2015). It has to be noted that these values are optimized towards their modern distribution and that this is strongly dependent on the assumption that the climatic range of the fossil taxon is the same as the modern taxon (Utescher et al. 2014). It is possible that the modern distribution is a function of its past climatic or biogeographic history, instead of its modern climatic tolerance (e.g. Reichgelt et al. 2016); however, the uncertainty inherent in assuming that the modern represents past climatic range can be minimized by incorporating as many taxa as possible (Harbert and Nixon 2015).

In this study we constrained bioclimatic envelopes by linking climatic variables, i.e. under the assumption that taxa occurrences in a location are dependent on all climatic factors combined, rather than each factor separately. Calculating bioclimatic envelopes separately can lead to the inclusion of apparent coexistence intervals, in which no modern occurrence is recorded, but can wrongfully be included in the bioclimatic envelope (Grimm and Potts 2016). To avoid this problem, we calculated the probability density of taxa co-occurrence for each combination of MAT, ST, WT, MAP, SP and WP. First, the likelihood (f) of a taxon (t) occurring at value (x) for a certain climatic variable is calculated using the mean (μ) and standard deviation (σ) of the modern distribution range (Table 1) of that taxa (Eq. (1)).

$$f(x) = \frac{1}{\sqrt{2\sigma^2\pi}} e^{-\frac{(x-\mu)^2}{2\sigma^2}} \quad (1)$$

This likelihood is then combined with likelihood calculations for that taxon's occurrence at a recorded combination of climatic variables (Eq. (2)).

$$f(t) = f(x_1) \times f(x_2) \ldots \times f(x_n) \quad (2)$$

Finally, the likelihood is then combined with likelihood calculations for all taxa in a specific assemblage, to arrive at a single probability that a particular combination of taxa may occur at a particular combination of climatic variables (Eq. (3)).

$$f(z) = f(t_1) \times f(t_2) \ldots \times f(t_n) \quad (3)$$

This analysis provides normally distributed probability density functions of a taxon's relation to climate but allows for a calculation of likelihood of a combination of climatic variables. The occurrence of a taxon along a climatic gradient can have widely variable levels of probability (Fig. 4) and through our method, this uncertainty is incorporated into the results. Different taxon combinations may result in strongly varying levels of probability. Therefore, to allow cross-comparison of probabilities between samples, a relative probability for each climatic combination for each sample was calculated, standardized to the highest absolute probability (Eq. (4)).

$$f(z)_{rel} = f(z) \Big/ f(z)_{max} \quad (4)$$

Some taxa were excluded from the analysis because of the ambiguity of their climatic relevance. The needle-leaf conifers *Abies*, *Pinus* and *Picea* (all members of the Pinaceae) have wind-dispersed pollen and are known to contribute significantly to background pollen rain in a marine setting (Hooghiemstra 1988; Mudie and McCarthy 1994).

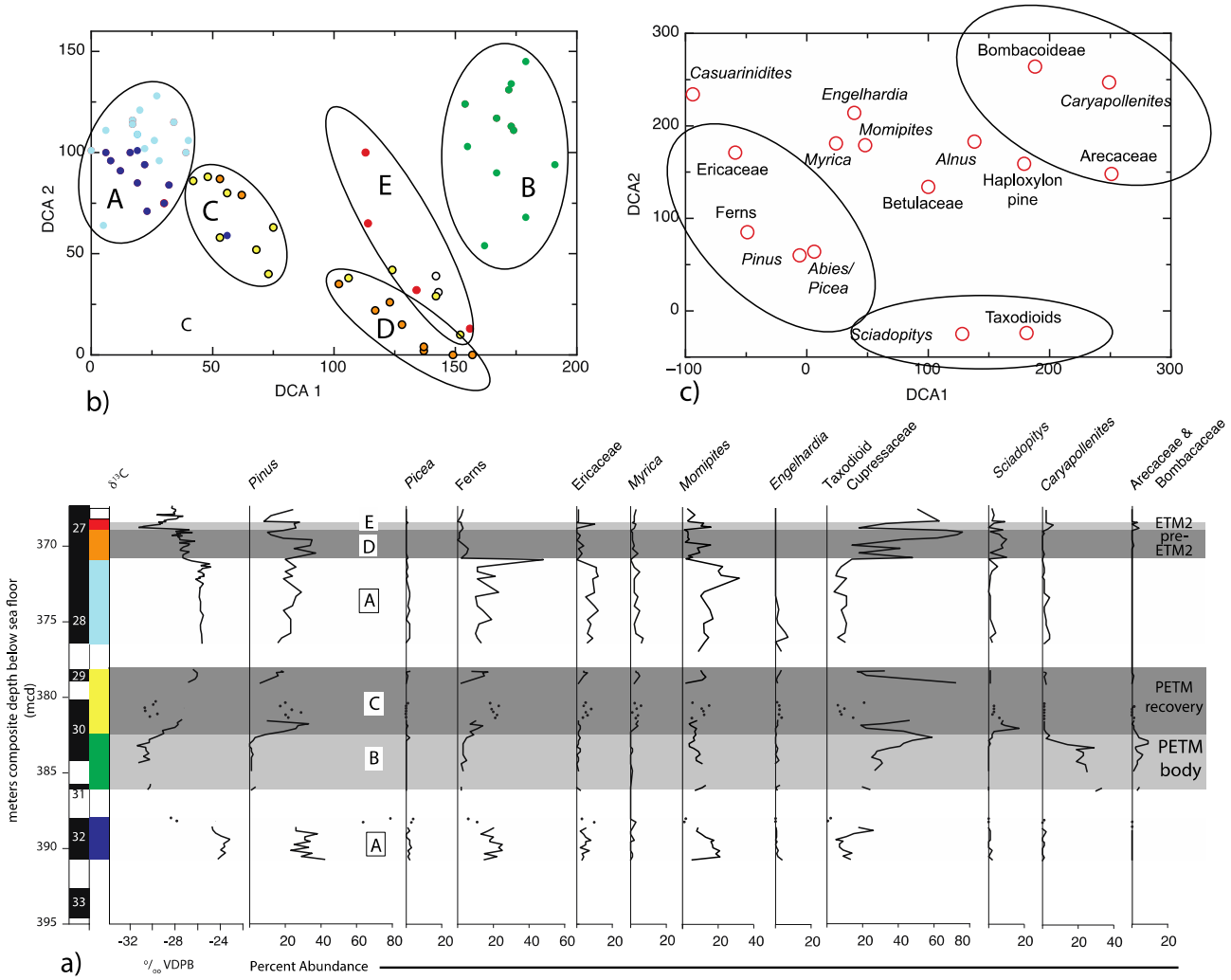

Fig. 2. (a) Carbon isotope curve (Sluijs et al., 2009) and percent abundance of pollen from major plant taxa, IODP Site 302-4A, central Arctic Ocean. Cores 27–33 represent the late Paleocene through early Eocene interval, and white segments indicate intervals of no core recovery. White shading (A) represents background (non-hyperthermal) periods. Light gray shading (B and E) indicates hyperthermal events (PETM from 387 to 378.5 mcd and ETM2 event from 368.7 to 368.2 mcd). Dark gray shading (C) represents the PETM recovery phase (383.03–378.5 mcd), and dark gray shading (D) represents the pre-ETM2 interval (371–368.94 mcd). (b) Plot of Detrended Correspondence Analysis (DCA) analyses of samples in Fig. 2a (DCA axis 1 vs. DCA axis 2). Colored dots are keyed to corresponding intervals in Fig. 2a. (c) Plot of DCA of major taxa.

Although pollen dispersal models indicate that *Picea* and *Abies* are poorly dispersed relative to *Pinus* (Jackson and Lyford 1999), morphological adaptations of bisaccate pollen to long-distance transport by wind and water generally result in the relative increases in abundance with increased distance from shore (Mudie and McCarthy 2006). The angiosperms Asteraceae, Cyperaceae, Ericaceae, Gentianaceae, Liliaceae, Onagraceae and Poaceae have a very wide climatic range today (polar to tropical), although lower taxonomic units within these families can have very strong climatic specificity. The inclusion of climatically ambiguous taxa biases the probability density analysis towards a single mean. For lack of intrafamiliar taxonomic assignment, these plant families were omitted from the analysis as well. Modern-day *Sciadopitys* has a relict distribution in Japan. It was much more widely dispersed and may have occupied a larger climatic range in the past (e.g. Mosbrugger et al. 1994). The ± 2 σ range was used in place of the ± 1 σ range in our analysis to accommodate this uncertainty. Similarly, we used the ± 2 σ range in place of the ± 1 σ range for the broadleaf trees *Acer*, *Alnus*, *Betula*, *Castanea*, *Corylus*, *Fraxinus*, *Myrica*, *Carpinus/Ostrya*, *Salix*, *Tilia* and *Ulmus*, because these taxa tend to be oversampled in the cool-temperate and continental environments of Europe and North America, and these taxa are more likely to have tended towards warmer climates in the early Cenozoic (Eberle and Greenwood 2012; Greenwood et al. 2005).

2.4. Lipid biomarker analysis

BrGDGTs are bacterial membrane lipids that have been found in soils and peats worldwide. Their relative distribution has been demonstrated to respond to mean air temperature, and forms the basis for the use of brGDGTs as continental paleothermometers (Weijers et al. 2007a; De Jonge et al. 2014). Upon soil mobilization and runoff, brGDGTs can be transported by rivers to the marine environment, where their incorporation in the sedimentary record results in a climate archive of the adjacent land (Weijers et al. 2007b). BrGDGTs were analyzed in the polar fractions previously generated by Sluijs et al. (2006, 2009). In short, freeze-dried and homogenized sediments were extracted with a Dionex Accelerated Solvent Extractor using a mixture of dichloromethane (DCM):MeOH 9:1 (*v*/v). Total lipid extracts were separated into an apolar and polar fraction over an Al_2O_3 column using hexane:DCM 9:1 (v/v) and DCM:MeOH 1:1 (v/v) as eluents, respectively. Polar fractions, containing the brGDGTs, were dissolved in hexane:isopropanol 99:1 (v/v) and filtered over a 0.45 µm PTFE filter

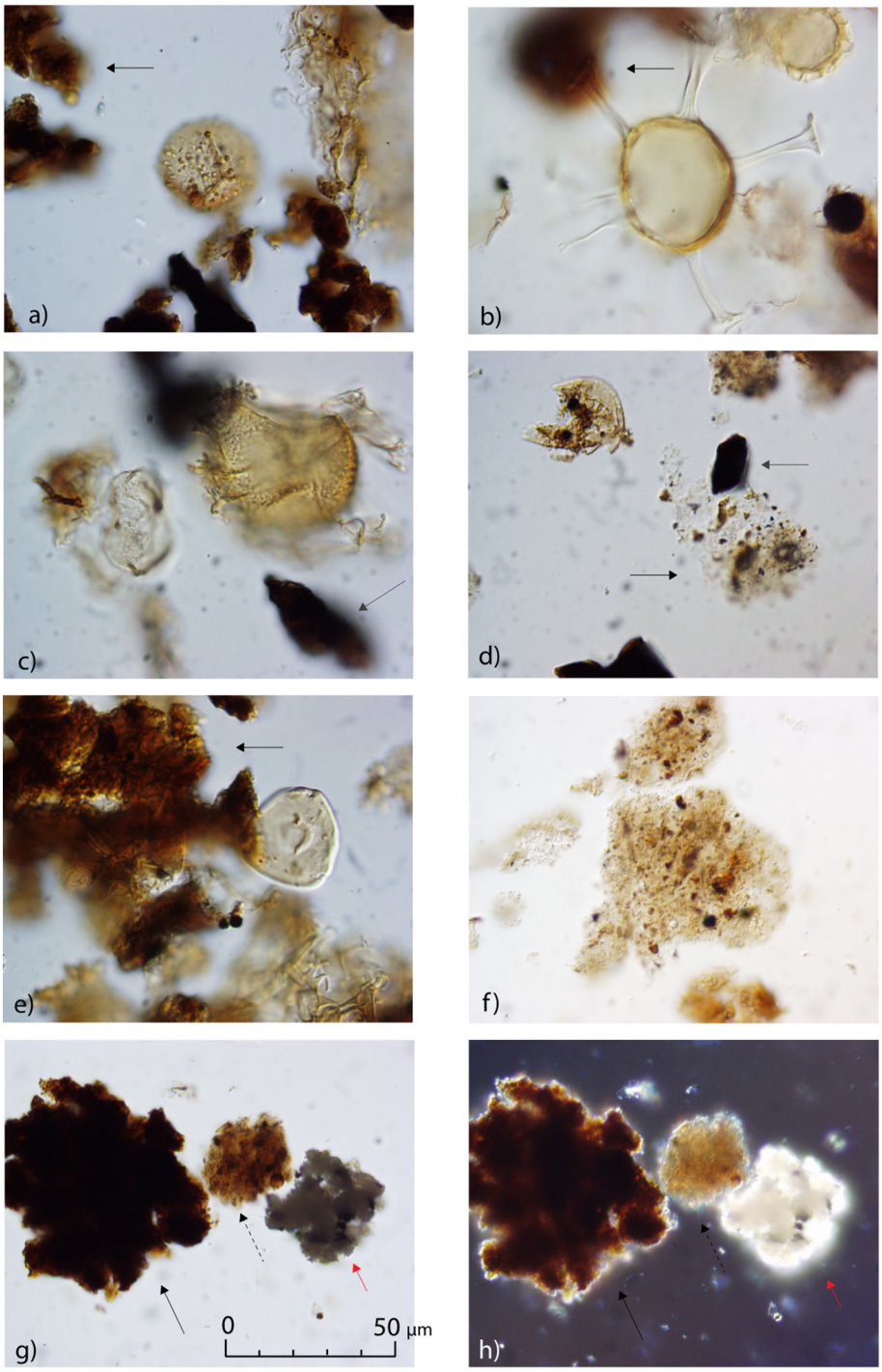

Fig. 3. Illustrations of palynomorphs from IODP Site 302-4A, Lomonosov Ridge, central Arctic Ocean. The scale in 3 g applies to all photographs. (a) Massive Amorphous Organic Matter (AOM) (black arrow) and spore from ETM2, 368.79 mcd (IODP 302-4A-27X-1, 139–141 cm); (b) Dinocysts and massive AOM (black arrow), pre-ETM2 interval, 371 mcd (IODP 302-4A-27X-3, 60–62 cm); (c) Dinocysts and angular opaque fragments (gray arrow), post-PETM interval, 372.67 mcd (IODP 302-4A-28X-1, 40–42 cm); (d) Granular AOM (black arrow), Cupressaceae pollen, and angular opaque fragment (gray arrow) from PETM recovery interval, 381.93 mcd (IODP 302-4A-30X-2, 1–3 cm); (e) *Caryapollenites* and massive AOM (black arrow) from peak PETM interval, 384.34 mcd (IODP 302-4A-30X-3, 101–103 cm); (f) Granular AOM from late Paleocene sediments, 389.21 mcd (IODP 302-4A-32X-2, 121–123 cm); (g) Massive AOM (black arrow), granular AOM (dashed arrow), and fluorescent AOM (red arrow) from late Paleocene sediments, 389.21 mcd (IODP 302-4A-32X-2, 121–123 cm); (h) same image as in (g) photographed under Nomarski dark field, showing brightness of fluorescent AOM.

prior to analysis using ultra-high performance liquid chromatography mass spectrometry (UHPLC-MS) on an Agilent 1260 infinity series instrument coupled to a 6130 quadrupole mass selective detector at Utrecht University, with settings according to Hopmans et al., 2016. BrGDGTs were separated over two silica Waters Acquity UPLC HEB Hilic (1.7 µm, 2.1 × 150 mm) columns in tandem, preceded by a guard column (2.1 × 5 mm) packed with the same material. BrGDGTs were eluted isocratically for 25 min with 18% B at a flow rate of 0.2 ml/min, followed by a linear gradient to 30% B in 25 min, and then to 100% B in 30 min, where A is hexane and B is hexane:isopropanol 9:1 (v/v). BrGDGTs were ionized using atmospheric pressure chemical ionization, after which $[M + H]^+$ were detected in selected ion monitoring mode.

MAT was calculated using fractional brGDGT abundances and the transfer function based on the global surface soil calibration dataset of De Jonge et al. (2014). The analytical uncertainty on brGDGT-based MAT estimates is < 0.5 °C based on long-term measurements of in-house standards. The uncertainty on the calibration, however, is 4.6 °C (De Jonge et al. 2014). Nevertheless, the scatter in the calibration is considered to be mainly systematic and can be attributed to the heterogeneity of soils in the global calibration set and accompanying spread in environmental parameters other than temperature. As such, the uncertainty is likely much smaller when the brGDGT proxy is applied on a smaller scale. The remaining uncertainty then applies to the record as a whole (i.e. the record can shift up and down a few degrees), but the timing and direction of changes in the brGDGT record are robust.

Table 1
Means and standard deviations used in our bioclimatic analysis probability density model.

Taxon	MAT (°C)	1σ	ST (°C)	1σ	WT (°C)	1σ	log MAP (mm)	1σ	log SP (mm)	1σ	log WP (mm)	1σ
Acer	9	**5**	16.6	**4.9**	1.5	**7.1**	2.91	0.1	2.32	0.2	2.28	0.2
Alnus	8.4	**5.2**	15.7	**4.2**	1.3	**7.4**	2.9	0.1	2.31	0.1	2.28	0.2
Anemia	21	3	23.5	2.8	18.1	3.7	3.17	0.1	2.63	0.2	2.24	0.4
Arecoideae/Trachycarpeae	22.3	4.5	25.1	3.5	19.2	6	3.17	0.2	2.53	0.4	2.18	0.7
Betula	7	**5.7**	15.7	**4.6**	−1.7	**8.8**	2.87	0.1	2.33	0.1	2.21	0.2
Bombacoideae	26.5	1.9	28.6	2.1	24.2	2.3	3.15	2.7	2.45	0.3	1.6	1
Carya	12.9	4.4	22.9	3	2.1	6.6	3	0.1	2.44	0.2	2.27	0.3
Castanea	10.4	**3.5**	17.3	**4.2**	3.6	**4.1**	2.91	0.1	2.27	0.2	2.31	0.1
Casuarina	18.2	2.5	23.9	2.3	12	3.3	2.78	0.3	2.24	0.4	2.05	0.3
Celtis	19.7	5.8	24.6	3.6	14.3	8.6	3.02	0.2	2.43	0.4	1.99	0.6
Corylus	8.8	**3.8**	16	**3.5**	1.7	**5.4**	2.9	0.1	2.31	0.1	2.29	0.2
Engelhardia	19.4	2.8	23.1	2.8	14.8	3.3	3.43	0.1	3.05	0.2	2.32	0.3
Fraxinus	9.2	**4**	16.1	**4.3**	2.5	**5.6**	2.91	0.1	2.29	0.2	2.3	0.2
Gleichenia	16.9	6	19.9	5	13.6	7	3.28	0.2	2.61	0.4	2.58	0.3
Ilex	17.3	5.7	22.4	4.3	11.8	8.7	3.2	0.2	2.67	0.3	2.26	0.5
Lycopodium	6.3	4.2	14.6	3.1	−1.8	6.2	2.95	0.2	2.41	0.2	2.28	0.3
Morus	16	4.4	23.6	3.5	7.9	7.1	3.13	0.2	2.66	0.3	2.2	0.4
Myrica	7	**5**	15.3	**3.7**	−1.1	**7.5**	2.9	0.1	2.34	0.1	2.25	0.2
Myriophyllum	8.6	4.5	16.2	3.4	1.2	6.2	2.88	0.2	2.3	0.2	2.24	0.3
Nymphaea	10.4	5.9	17.2	4.3	3.6	7.6	2.92	0.2	2.34	0.2	2.21	0.4
Nyssa	14.1	4.4	23.7	3.1	3.8	6.1	3.1	0.1	2.55	0.1	2.39	0.2
Osmundaceae	10.6	3.4	17	3.3	4.2	4.8	3.06	0.2	2.44	0.3	2.43	0.3
Carpinus + Ostrya	9.4	**3.8**	17.1	**3.5**	1.6	**5.3**	2.89	0.1	2.35	0.1	2.23	0.1
Plantago	9.3	3.7	16.7	3	2.1	4.9	2.87	0.1	2.26	0.2	2.24	0.2
Platanus	13.5	3.7	21.6	3.1	5.3	5.7	2.87	0.2	2.04	0.6	2.26	0.3
Platycarya	16.1	3.1	23.9	3.8	7.6	3.9	3.2	0.2	2.81	0.1	2.13	0.3
Pterocarya	14.1	4.3	23	3.6	4.6	5.2	3.14	0.2	2.71	0.2	2.1	0.4
Quercus	11.2	**6.4**	18.7	**7**	4.2	**7.1**	2.85	0.1	2.08	0.4	2.26	0.2
Sagittaria	10.1	4.5	17.8	3.4	2.2	6.2	2.88	0.1	2.32	0.2	2.21	0.2
Salix	7.8	**7.1**	15.2	**5.9**	0.6	**9.4**	2.9	0.1	2.3	0.2	2.28	0.2
Sciadopitys	11.2	**4.8**	21.8	**4.5**	0.7	**5.7**	3.26	0.1	2.81	0.1	2.37	0.2
Selaginella	9.6	8.7	16.1	6.4	3.3	11.2	3.02	0.3	2.39	0.4	2.33	0.4
Sparganium	7.5	2.6	15.4	1.6	−0.2	4.2	2.86	0.1	2.3	0.1	2.22	0.2
Sphagnum	6.1	3.6	13.7	2.1	−1	5.9	2.96	0.2	2.37	0.1	2.35	0.2
Symplocos	18	4.5	22.2	4.3	13.3	6.5	3.25	0.2	2.78	0.2	2.29	0.4
Taxodioid Cupressaceae	15.1	4.5	21.4	5.2	8.6	5.1	3.07	0.2	2.25	0.6	2.31	0.4
Tilia	7.7	**5.1**	16.2	**3.7**	−0.6	**7.7**	2.86	0.1	2.31	0.1	2.2	0.2
Trachycarpeae/*Phoenix*	21.4	5	25.7	3.4	16.8	6.6	2.99	0.3	2.26	0.6	1.83	0.7
Tsuga	8.3	3.7	17.9	3.7	−1.7	5.6	3.09	0.2	2.44	0.3	2.39	0.4
Ulmus	8.9	**5**	16	**4.9**	2	**6.4**	2.9	0.1	2.29	0.2	2.29	0.2

Bolded values indicate where the ± 2σ range was used instead of the ± 1σ range.

3. Results

3.1. Pollen assemblages

Five distinct assemblages of pollen and spore data are represented in the late Paleocene through early Eocene of the ACEX site (Fig. 2). Mixed conifer-broadleaved forests (Fig. 2, group A) likely occupied upland areas on land masses near the ACEX core site before and after the hyperthermal events and represent the background (non-hyperthermal) vegetation signature. These assemblages are dominated by wind-dispersed conifers, pine and spruce (*Pinus*, *Picea*), with common pollen of broadleaf trees such as the walnut family (Juglandaceae) and the rhododendron/heath family (Ericaceae), and also fern spores.

Mixed forests with abundant needle-leaved taxa, (Fig. 2, groups C and D) indicative of fluvial wetlands and other lowlands, dominated during the PETM recovery and pre-ETM2 interval (383.03–378.5 mcd and 371–368.94 mcd, respectively; Fig. 5). Both groups C and D are dominated strongly by taxodioid Cupressaceae (represented by papillate grains attributable to *Metasequoia*, *Taxodium*, and other taxodioid taxa), but they differ in the relative abundance of fern spores and *Sciadopitys* pollen.

The hyperthermal events (PETM: ~387–378.5 mcd; ETM2:

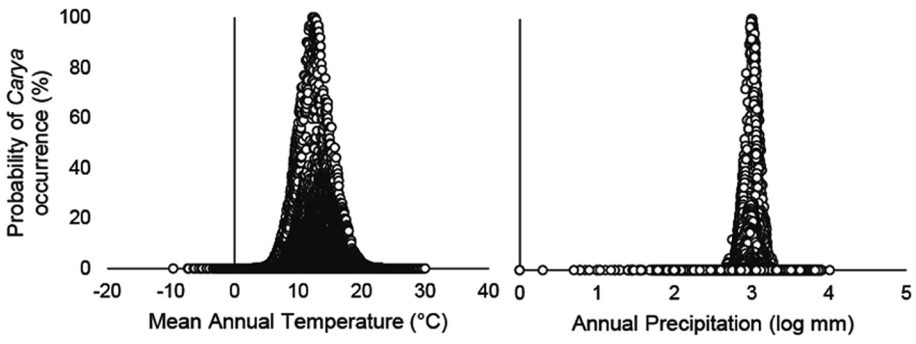

Fig. 4. Example of probability density distribution of a taxon based on the data in Table 1 and calculated using Formulas (1) and (2).

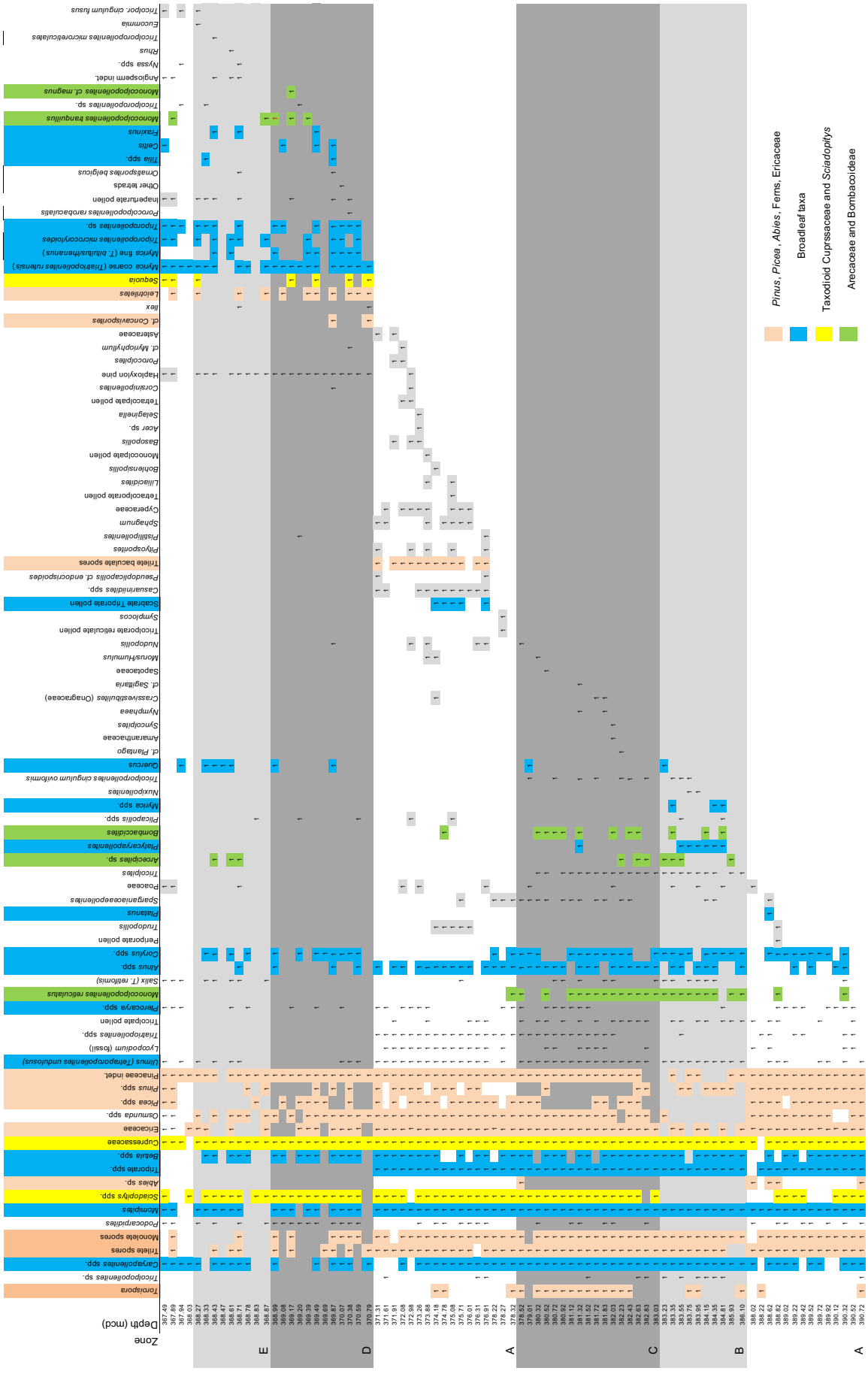

Fig. 5. Stratigraphic distribution of pollen and spore taxa vs. depth in IODP 302-4A. The number "1" indicates the presence of a taxon in a given sample. White shading (A) represents background (non-hyperthermal) periods. Light gray shading (B and E) indicates hyperthermal events (PETM from 387 to 378.5 mcd and ETM2 event from 368.7368.2 mcd). Dark gray shading represents the PETM recovery phase (C: 383.03–378.5 mcd) and the pre-ETM2 interval (D: 371–368.94 mcd). Orange shading highlights occurrence of *Pinus*, *Picea*, *Abies*, ferns, and Ericaceae pollen; blue shading highlights occurrence of pollen of broadleaf trees; yellow shading highlights occurrence of taxodioid Cupressaceae and *Sciadopitys* pollen; and green shading highlights occurrence of Arecaceae, Bombacoideae, and other monosulcate pollen grains. (For interpretation of the references to colour in this figure legend, the reader is referred to the web version of this article.)

368.94–368.2 mcd) are characterized by pollen assemblages representative of broad-leaved swamp forests (Fig. 2, groups B and E). These assemblages are characterized by higher abundance of *Caryapollenites* (Juglandaceae; likely *Carya*, extant hickory and pecan), common occurrence of taxodioid Cupressaceae, and presence of mesothermal to megathermal Arecaceae (palm family) and Bombacoideae (balsa, baobab subfamily) (Fig. 5; Fig S1). Peak PETM assemblages (group B) differ from those of the ETM2 (group E) in much higher abundances of *Caryapollenites* and much lower abundances of *Pinus* pollen.

3.2. Quantitative paleoclimate reconstructions

3.2.1. Bioclimatic analysis

The bioclimatic analyses provide estimates of mean annual temperature (MAT), summer and winter average temperatures (ST [JJA] and WT [DJF], respectively), mean annual precipitation (MAP), and summer and winter precipitation (SP and WP, respectively). Our NLR-based MAT estimates show a generally warm (upper microthermal to mesothermal: 13–20 °C; sensu Wolfe, 1979) terrestrial temperature range of 10–17 °C for the late Paleocene through ETM2 interval. A substantial MAT increase occurred during the PETM peak (15.0 + 1.9/−2.1 °C; Fig. 6), compared to late Paleocene background temperatures (12.9 + 1.1/−1.2 °C; Table 2). MAT decreased during the PETM recovery (14.3 + 1.8/−1.9 °C), remaining warmer than the late Paleocene baseline of 12.9 °C. Cooling continued during the post-PETM interval (13.9 + 1.0/−1.1 °C). MAT decreased during the transition into the ETM2 (12.7 + 1.9/−2.1 °C), with further cooling during the ETM2 (12.3 + 2.3/−2.5 °C; Fig. 6). In the two samples above the ETM2, MAT decreased further to lower than late Paleocene background values.

Seasonal temperature reconstructions show that the warming was primarily a winter phenomenon, with little variability in summer temperatures throughout the entire study interval (Fig. 6). NLR reconstructions suggest that winter temperatures (WT) during the PETM (9.3 + 2.2/−2.6 °C) were an average of ~2 °C warmer than the late Paleocene (6.8 + 1.6/−1.9 °C) and cooling set in after the event (PETM recovery: 8.6 + 2.2/−2.4 °C and post PETM: 8.3 + 1.2/−1.4 °C; Table 2). Average WTs decreased by > 2 °C in the pre-ETM2 (6.2 + 2.5/−3.0 °C), decreasing further during the ETM2 (5.4 + 3.0/−3.3 °C). Although the average WT for the ETM2 is 5.4 °C, this is skewed by a single value of 11.6 °C, with the remaining five samples ranging from 2.6 to 5.9 °C. The generally low estimates of cool ETM2 winter temperatures contrast with the presence of palm and Bombacoideae pollen, which suggests that winter temperatures were at least 5–10 °C during the hyperthermals (Pross et al. 2012; Reichgelt et al. 2018).

Reconstructed mean annual precipitation (MAP) values are moderately high (> 800 mm yr^{-1}) throughout the interval, although there are large uncertainties in these estimates (late Paleocene: 952 + 84/

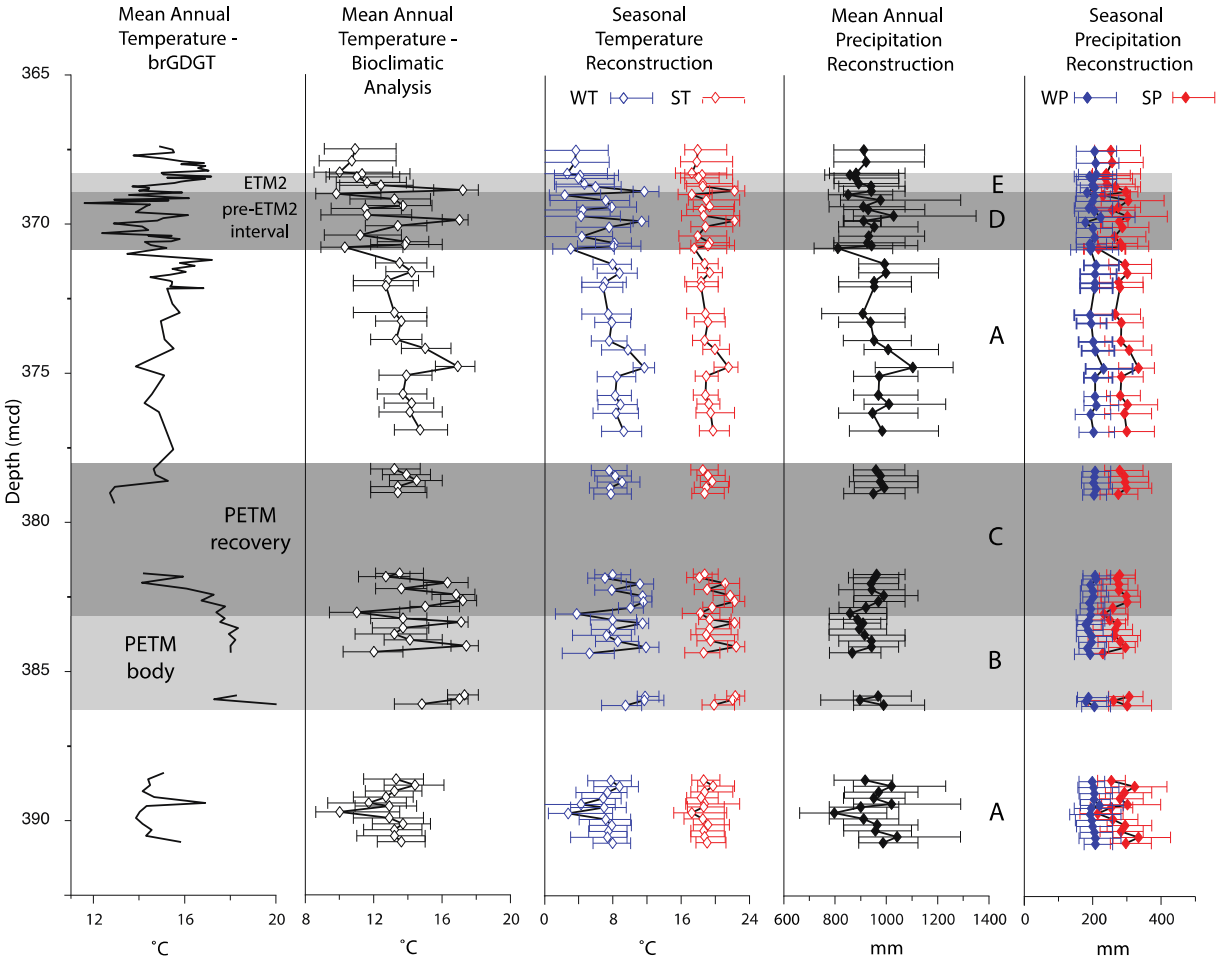

Fig. 6. Temperature estimates from lipid biomarkers (brGDGT) and bioclimatic estimates from IODP 302-4A, central Arctic Ocean. brGDGT estimates of Mean Annual Temperature are based on a transfer function (De Jonge et al. 2014). Mean Annual Temperature (MAT), ST, WT, MAP, SP, and WP) are based on Bioclimatic Analyses. White shading (A) represents background (non-hyperthermal) periods. Light gray shading (B and E) indicates hyperthermal events (PETM from 387 to 378.5 mcd and ETM2 event from 368.7368.2 mcd). Dark gray shading (C) represents the PETM recovery phase (383.03–378.5 mcd), and dark gray shading (D) represents the pre-ETM2 interval (371–368.94 mcd).

Table 2
For each interval in the ACEX late Paleocene – early Eocene section, the range and average of estimates of Mean Annual Temperature (MAT) (both Bioclimatic and brGDGT estimates) and Summer Temperature (ST), Winter Temperature (WT), Annual Precipitation (AP), Summer Precipitation (SP), and Winter Precipitation (WP) from bioclimatic estimates.

Interval	Depth range (mcd)	Bioclimatic estimates							brGDGT estimates	
		n	MAT (°C) range and average	ST (°C) range and average	WT (°C) range and average	AP (mm) range and average	SP (mm) range and average	WP (mm) range and average	n	MAT (°C) range and average
Post – ETM2	**368.23–367.40**	2	10.7–10.9 **(10.8)**	17.8–17.9 **(17.9)**	3.5–3.6 **(3.5)**	911–920 **(916)**	252–256 **(254)**	205–208 **(207)**	13	13.7–17.0 **(15.9)**
ETM2	**368.94–368.28**	6	10.0–22.2 **(12.3)**	17.2–22.2 **(18.8)**	2.6–11.6 **(5.4)**	857–940 **(898)**	236–296 **(253)**	183–210 **(198)**	15	13.7–17.2 **(15.2)**
Pre-ETM2	**370.79–369.02**	11	9.8–17.0 **(12.7)**	17.2–22.2 **(18.8)**	2.3–11.3 **(6.2)**	810–1027 **(923)**	216–303 **(270)**	178–222 **(198)**	25	11.6–16.2 **(14.4)**
Post PETM	**378.22–371.20**	15	12.7–16.9 **(14.0)**	18.3–21.5 **(19.2)**	6.8–11.6 **(8.4)**	907–1102 **(975)**	265–333 **(291)**	192–231 **(205)**	28	13.5–17.2 **(15.2)**
PETM recovery	**383.03–378.5**	11	11.0–17.2 **(14.4)**	18.1–22.2 **(19.6)**	3.7–11.5 **(8.8)**	857–991 **(949)**	232–300 **(285)**	190–209 **(202)**	11	12.7–17.8 **(15.5)**
PETM body	**386.1–383.23**	10	12.1–17.4 **(14.7)**	18.6–22.4 **(20.2)**	5.2–11.8 **(8.9)**	866–988 **(920)**	229–306 **(268)**	179–204 **(190)**	10	17.3–20.0 **(18.1)**
Late Paleocene	**390.72–388.62**	12	10.0–14.4 **(12.9)**	17.2–19.7 **(18.6)**	2.7–8.7 **(6.8)**	796–1041 **(952)**	214–333 **(282)**	192–219 **(202)**	12	13.9–16.9 **(14.6)**

Average values are presented parenthetically in bold font.

$-72\,mm\,yr^{-1}$, PETM body: $920 + 52/-48\,mm\,yr^{-1}$, PETM recovery: $949 + 48/-44\,mm\,yr^{-1}$, post PETM: $975 + 63/-53\,mm\,yr^{-1}$, pre-ETM2: $923 + 86/-60\,mm\,yr^{-1}$ and ETM2: $898 + 50/-41\,mm\,yr^{-1}$). These reconstructions show little variability and suggest that precipitation variability during hyperthermal events was only a secondary driver of vegetation during this period.

3.2.2. Lipid-biomarker estimates of mean annual temperature

BrGDGTs are present throughout the studied interval. Although they were initially thought to be solely produced in soils, recent studies indicate that brGDGTs may also be produced in the coastal marine environment, altering the initial soil-derived temperature signal (Peterse et al. 2009; Sinninghe Damsté 2016). Based on a comparison of brGDGT signatures in modern shelf sediments and soils, the weighted average number of rings in the tetramethylated brGDGTs ($\#rings_{tetra}$) has been proposed to identify a possible marine overprint (Sinninghe Damsté 2016). The $\#rings_{tetra}$ is defined as:

$$([brGDGT{-}Ib] + 2^{*}[brGDGT{-}Ic])/([brGDGT{-}Ia] + [brGDGT{-}Ib] + [brGDGT{-}Ic])$$

In which Roman numerals refer to the brGDGT structures in De Jonge et al. 2014.

Sinninghe Damsté (2016) showed that the $\#rings_{tetra}$ in near coastal shelf sediments is similar to that in soils, in agreement with their soil-origin, but then increases towards the open ocean, indicating a contribution from in situ produced brGDGTs. In particular, the zone from 50 to 300 m water depth appears favourable for marine brGDGT production. The maximum $\#rings_{tetra}$ of 1 is observed in Svalbard fjord sediments where soil input is negligible, and is considered as an end-member for a purely marine origin of the brGDGTs. On the other hand, the $\#rings_{tetra}$ in the soils from the global calibration dataset is always < 0.7, which has consequently been proposed as the threshold value indicating a mixed source of the brGDGTs (Sinninghe Damsté 2016). In our record, $\#rings_{tetra}$ is always below 0.21, which is well below this threshold, supporting a primary soil source of the brGDGTs at this site and thus their suitability to serve as continental paleothermometer.

Our resulting MAT record indicates a warm (upper microthermal - lower mesothermal) climate, with temperatures ranging from 13 to 20 °C (Table 2) from the late Paleocene through the ETM2. Reconstructed mean annual temperatures in the PETM body (18.1 °C) averaged 3.5 °C warmer than average background values (14.6 °C) of the late Paleocene (Fig. 6). During the PETM recovery, the average MAT decreased to a post-PETM level of 15.5 °C, with the gradual temperature decrease mirroring the CIE. The brGDGT data suggest that pre-ETM2 temperatures decreased slightly by an average of 0.8 °C (Fig. 6) before warming again during the ETM2 to an average of 15.2 °C, with peak temperatures occurring in the upper 40 cm of the unit (Fig. 6). The brGDGT estimates of MAT for the post-ETM2 unit remained high, decreasing slightly in the uppermost samples.

3.2.3. Comparison of bioclimate and lipid-biomarker estimates of mean annual temperature

Both bioclimatic and brGDGT reconstructions of MAT indicate the occurrence of warm climates throughout late Paleocene to early Eocene time, with brGDGT estimates typically warmer than NLR-based bioclimate estimates. The two methods show similar patterns surrounding the PETM interval: warming from the late Paleocene into the PETM body; cooler PETM recovery, and further cooling during the post-PETM interval. Although both methods indicate continued cooling into the pre-ETM2 interval, they differ during the ETM2 interval. The brGDGT-based estimates indicate an average warming of 0.8 °C, whereas bioclimatic estimates indicate little change or a slight cooling during the ETM2 (Fig. 6; Table 2). The enhanced warmth reconstructed by brGDGT vs. bioclimatic methods was most notable during the PETM,

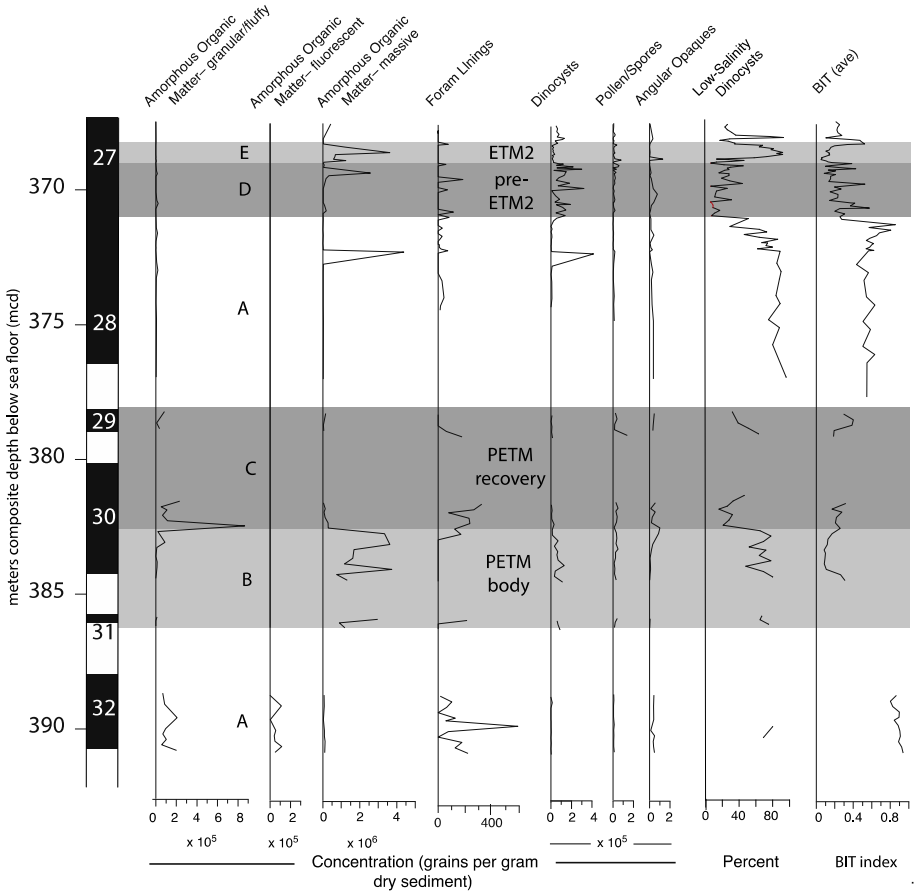

Fig. 7. Concentration of particulate organic matter quantified during palynofacies analysis: Amorphous Organic Matter (AOM), and angular opaque particles (this study); foraminiferal lining, dinocyst and pollen/spore concentrations (Sluijs et al. 2009, 2006); and BIT index (Sluijs et al. 2009). White shading (A) represents background (non-hyperthermal) periods. Light gray shading (B and E) indicates hyperthermal events (PETM from 387 to 378.5 mcd and ETM2 event from 368.7368.2 mcd). Dark gray shading (C) represents the PETM recovery phase (383.03–378.5 mcd), and dark gray shading (D) represents the pre-ETM2 interval (371–368.94 mcd).

when individual brGDGT estimates exceed those based on bioclimatic analyses by as much as 6 °C.

3.3. Palynofacies analysis

Late Paleocene palynofacies are dominated by granular/fluffy AOM and fluorescent AOM, common occurrence of massive AOM and angular opaque material (Fig. 7). Pollen/spores of terrestrial plants and dinocysts are present in low concentrations in this unit; bisaccate pollen grains are the dominant element of terrestrial pollen/spore assemblages, and low-salinity dinocysts dominate the sparse algal assemblages.

Concentrations of massive AOM increased nearly twenty-fold in the PETM body. Concentrations of both pollen/spores and dinocysts also increased, with dinocyst concentrations about twice those of pollen/spores (Fig. 7). Fluorescent AOM was absent, and granular AOM was rare. Low-salinity taxa continued to dominate dinocyst assemblages (Sluijs et al. 2006), and pollen assemblages were dominated by angiosperms. During the PETM recovery, concentrations of massive AOM decreased and granular/fluffy AOM increased to late Paleocene levels. Although pollen/spore concentrations maintained similar concentrations to the PETM body, dinocyst concentrations decreased significantly, and assemblages in the early recovery phase were dominated by dinocyst taxa characteristic of normal marine salinities (Sluijs et al. 2006).

Aside from one peak in massive AOM and aquatic palynomorphs at 372.22 mcd, all palynomorphs were present in very low concentrations in the post-PETM (Fig. 7). Low-salinity taxa dominated dinocyst assemblages during this interval (Sluijs et al. 2006). At the onset of the pre-ETM2 interval at 371 mcd, dinocyst concentration quadrupled, and the proportions of normal marine dinocysts increased sharply, concurrent with a decrease in BIT that has been interpreted as a transgressive signal (Sluis et al., 2008). The ETM2 was characterized by an average ten-fold increase in concentration of massive AOM, reduced dinocyst concentrations, and dominance of low-salinity dinocyst taxa (Sluijs et al. 2009). Above the ETM2, normal marine dinocysts returned to dominance, dinocyst concentration doubled, and pollen/spores, and massive AOM returned to low concentrations.

4. Discussion

4.1. Late Paleocene vegetation and climate

Pollen evidence presented here indicates that mixed conifer-broadleaf forests occupied land masses near the ACEX site during the Late Paleocene. The relatively high percentages of bisaccate pollen (*Pinus*, *Picea*, *Abies*) suggests that conifer forests were present in upland sites; the common occurrence of Juglandaceae and taxodioid pollen and fern spores indicates that broadleaf forests and forested wetlands occurred near rivers and/or the coastline. Granular and fluorescent AOM overwhelmingly dominated late Paleocene palynofacies, and pollen, spores, and dinocysts were minor components of the assemblages. The dominance of AOM and presence of foraminifer linings (Fig. 7) are consistent with an aquatic/algal source for organic material (Batten 1983; Hart 1986; Wood and Gorin 1998) and deposition under hypoxic to anoxic, reducing conditions, possibly away from active sources of terrestrial organic matter (Batten 1996; Ercegovac and Kostić 2006; Harding et al. 2011; Tyson 1993). Increased fluorescence has been shown to be at least partially a result of microbial degradation (Pacton et al. 2011). The BIT indices for this interval are high (Fig. 7), which may reflect either an increased abundance of Crenarchaeotic bacteria due to fluctuating productivity or salinity stratification (Smith et al. 2012), high nutrient content (Buckles et al. 2016), or evidence for proximity to shore and high input of terrestrial material (Sluijs et al.

2006).

4.2. Arctic climate and vegetation during the Paleocene-Eocene Thermal Maximum

Although the onset of the PETM is absent from this record, meso- to megathermal taxa (palms/cycads and Bombacoideae) have been reported at other high-latitude sites during the peak carbon isotope excursion (CIE) (Eldrett et al. 2014; Schweitzer 1980). Our mean annual temperature reconstructions indicate an average warming of ~2 °C to 3.5 °C relative to the Late Paleocene, and winter temperatures are an average of 2 °C warmer (Table 2, Fig. 6). The presence of the meso- to megathermal taxa *Arecipites pseudotranquillus* (Arecaceae: Trachycarpeae), *Monocolpopollenites reticulatus* (Arecaceae: Arecoideae or Trachycarpeae) and *Bombaccidites* sp. (Bombacoideae) during the peak PETM (Fig. 5) indicates that cold-month mean temperatures (WT) during the hyperthermal were ≥5 °C (Greenwood and Wing 1995; Pross et al. 2012; Reichgelt et al. 2018). Palms and Bombacoideae currently are native to tropical and subtropical latitudes, although a few cold tolerant palm species extend as far as 44°N and 44°S (Dransfield et al. 2008; Greenwood and West, 2017; Reichgelt et al. 2018). Their presence in PETM sediments represents the northernmost occurrence of these taxa in the Paleocene and Eocene (Dransfield et al. 2008; Greenwood and Wing 1995; Sluijs et al. 2009; Suan et al. 2017; Trujillo 2009).

Although NLR estimates of PETM precipitation showed little difference from late Paleocene samples, the presence of meso- to megathermal taxa, which require greater moisture availability and longer growing season length (Blach-Overgaard et al. 2010; Walther et al. 2007) is suggestive of relatively wetter conditions. The striking increase in concentrations of massive AOM during the PETM (and ETM2), likely derived from terrestrial sources, may reflect the onset of reducing conditions and increased stratification of the water column (Fig. 7). Together with the absence of foraminiferal linings and dominance of low-salinity dinocyst species during this interval, increased fluvial discharge to the site is likely. Concentrations of dinocysts increased thirty-fold during the PETM peak CIE, and this apparent algal bloom may have been driven by an increased flux of terrestrial material and nutrients from the continent to the depositional site.

During the PETM recovery phase, mixed forests with abundant taxodioids (*Metasequoia*, *Taxodium*) replaced the broad-leaved forests, as mean annual temperatures decreased. The concentration of terrestrial AOM decreased to late Paleocene levels, and the concentration of granular AOM, typical of aquatic settings, increased. Combined with increased concentrations of foraminiferal linings and a shift to normal marine dinocyst species (Fig. 7) (Sluijs et al. 2006), these data indicate that riverine inputs decreased and that more typical marine conditions characterized the site during the recovery from the hyperthermal.

4.3. ACEX record of post-PETM vegetation and climate

Pollen assemblages reported here indicate a return to mixed conifer-broadleaf forests after the termination of the PETM (Fig. 5), and palynofacies analysis documents relatively low concentrations of all organic-walled microfossils. Within the pre-ETM2 interval (370.79–369.02 mcd), vegetation reverted to taxodioid-dominated forests, and dinocyst assemblages indicate normal marine conditions. Bioclimatic reconstructions of mean annual temperature indicate a slight cooling during this interval. During the ETM2, broadleaf forests with palms and Bombacoideae were present (Fig. 8). Combined with dinocyst evidence for low salinities and occurrence of massive AOM, our data suggest increased runoff from the continent to the site, reducing conditions, and, salinity stratification during the ETM2.

4.4. Comparison with other Paleocene and Early Eocene palynological records

Late Paleocene mixed conifer-broadleaf forests near the ACEX site included both upland (conifers such as pine, spruce, and fir; Pinaceae) and lowland elements representing forested wetlands with *Metasequoia*, *Taxodium,* ferns and broadleaf trees such as Juglandaceae. The occurrence of these assemblages at high latitudes indicates that the land surface from mid-latitudes of North America and Europe to the Arctic were covered by mixed conifer-broadleaf forests (Boulter and Manum 1989; Daly et al. 2011; Eldrett et al. 2014; Greenwood et al. 2010; Greenwood and Basinger 1994; Jolley et al. 2009; Jolley and Morton 2007; Jolley and Whitham 2004; Kender et al. 2012; Smith et al. 2007; Suan et al. 2017; West et al. 2015). Macrofloral data from Ellesmere Island (Fig. 1), while not clearly from the PETM and ETM2, show that the late Paleocene to early Eocene lowland terrestrial vegetation included coal-forming swamp forests dominated by conifers such as *Glyptostrobus* and *Metasequoia* (Cupressaceae), whereas upland forests were dominated by broadleaf taxa including Betulaceae, Cercidiphyllaceae/Trochodendraceae, Juglandaceae, Platanaceae, *Ulmus*, and *Tilia* (Eberle and Greenwood 2012).

The transition from the late Paleocene into the PETM was not recovered at the ACEX site, unlike sites from Spitsbergen, the North Sea, the mid-Atlantic coast of North America, and the U.K. (Eldrett et al. 2014; Harding et al. 2011; Kender et al. 2012; Self-Trail et al. 2017) (Fig. 1). Those sites indicate a warming event prior to the CIE onset, based on occurrence of *Apectodinium augustum* and increased abundance of pollen of broad-leaved taxa, and, in some sites, cycads or palms, which are characteristic of warmer climates (Reichgelt et al. 2018). At the onset of the CIE, there was a sharp and apparently short-lived increase in the abundance of fern spores, typically dominated by the fern spore *Cicatricosisporites* (Schizeaceae) and members of the Polypodiaceae (Collinson et al. 2009; Eldrett et al. 2014; Harding et al. 2011; Kender et al. 2012; Self-Trail et al. 2017). Combined with an increase in angiosperm diversity and greater abundance of marsh taxa such as *Typha*, these records indicate a rapid shift to wetter, warmer conditions and expansion of wetlands.

Vegetation during the PETM body at the ACEX site consisted of meso- to megathermal forests, including palms, members of the Bombacoideae and Juglandaceae (walnut family). A similar pattern was noted at the North Sea site, but palms were notably absent there during all but the very end of the PETM body. On the New Siberian Islands, palm pollen was present just before the onset of the PETM, mangrove pollen (*Avicennia*) occurred during the PETM, and dominance of taxodioid Cupressaceae pollen suggests the presence of forested wetlands in the region. Collectively, these data indicate the occurrence of mesothermal to megathermal taxa across the northernmost extent of landmasses during the PETM.

Needle-leaved mesic forests, dominated by *Metasequoia* and *Taxodium* as well as *Sciadopitys*, *Pinus* and ferns, characterize the PETM recovery at the ACEX site (Fig. 5). Few pollen records have been reported previously from the PETM recovery interval; although the Spitsbergen Gilsonryggen Member (Harding et al. 2011) contains sediments from the interval, pollen concentrations from these sediments were too low to report. Macrofossil records from the Big Horn Basin also indicate dominance of taxodioid conifers (Wing and Currano 2013) during the recovery, suggesting their occurrence from mid- to high-latitudes after the peak PETM.

Post-PETM assemblages are marked by the return of mixed conifer-broadleaf forests at the ACEX site. Cupressaceae were minor components, and pines, walnuts, Ericaceae and ferns were common. These assemblages were replaced by needle-leaf forests dominated by *Metasequoia*, *Taxodium* and *Sciadopitys* during the pre-ETM2 interval, which are similar to assemblages in the recovery phase of the PETM (Fig. 2). Meso- and megathermal elements (palms, Bombacoideae, *Carya*) occurred at the site during the ELMO event, but their pollen was

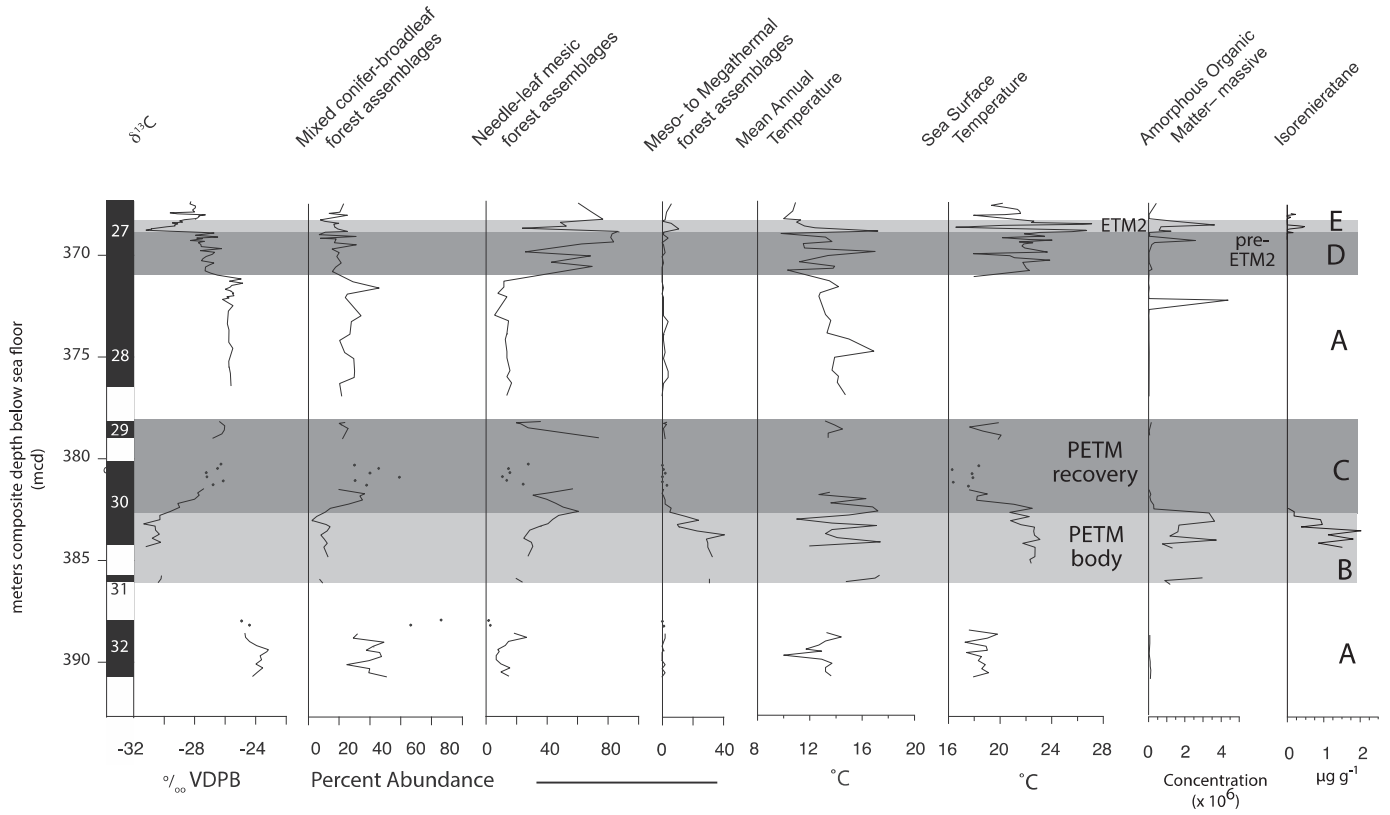

Fig. 8. Paleoclimate proxies from IODP 302-4A, central Arctic Ocean. Percent abundance of pollen groups, brGDGT and NLR estimates of Mean Annutal Temperature (this study); TEX86' estimates of sea surface temperatures and percentage of low-salinity dinocysts (Sluijs et al. 2009); and isorenieratane concentrations (Sluijs et al. 2006, 2009). White shading (A) represents background (non-hyperthermal) periods. Light gray shading (B and E) indicates hyperthermal events (PETM from 387 to 378.5 mcd and ETM2 event from 368.7–368.2 mcd). Dark gray shading (C) represents the PETM recovery phase (383.03–378.5 mcd), and dark gray shading (D) represents the pre-ETM2 interval (371–368.94 mcd).

less dominant than during the PETM.

4.5. Climatic implications of the ACEX records of Eocene hyperthermals

Analyses of palynological records of vegetation near the ACEX site provide insights into changing temperature and hydrology during Paleogene hyperthermals. The timing of pollen- and lipid-biomarker-based estimates of warmer mean annual temperatures during the peak PETM corresponds to warming sea surface temperatures, with comparable cooling during the PETM recovery (Fig. 8). Pollen-based bioclimatic estimates indicate that the ~2.4 °C increase in MAT was accompanied by winter temperature increases of ~2.5 °C and a more moderate increase in summer temperatures of 1.6 °C. Although bioclimatic reconstructions of late Paleocene to early Eocene precipitation show no notable change throughout the interval, increased precipitation and runoff from the continent is indicated by greater concentrations of palynomorphs and massive AOM. This observation is consistent with models and data suggesting greater moisture delivery to the Arctic at the beginning of the PETM, perhaps due to poleward migration of storm tracks and a reduced meridional temperature gradient (Pagani et al. 2006). The extremely high concentrations of AOM during the PETM are interpreted as representing increased microbial activity during hypoxic to anoxic conditions (Batten 1996; Tyson 1993), which is consistent with increased concentrations of isorenieratanes (biomarkers indicating anoxia) and lower salinity, based on heavier δD values during the hyperthermal (Pagani et al. 2006) (Fig. 8). During the PETM recovery, precipitation decreased, and ocean waters were more saline and oxygenated, based on vegetation changes, decrease in AOM concentrations, and a shift to normal marine dinocyst assemblages (Sluijs et al. 2006) (Fig. 8).

Vegetation and MAT during the pre-ETM2 interval indicate similar temperatures to the PETM recovery; surface salinities were high, and AOM concentrations were low until right before the ETM2. Coincident with the abrupt onset of the ETM2, the change to meso- to megathermal forests, high concentrations of AOM and isorenieratanes, and low-salinity dinocyst assemblages indicate a return to wetter conditions with increased continental runoff, stratification, and hypoxia during the ETM2 event. Although bioclimatic analyses do not show consistent warming during this interval, the presence of palms and Bombacoideae are suggestive of warmer conditions. Additionally, climate reconstructions based on leaf physiognomy from Ellesmere Island macrofloras (West et al. 2015) indicate the existence of micro- to mesothermal (MAT ~8–17 °C) and wet (MAP > 150 cm/yr) conditions, consistent with our climate reconstructions from the ACEX site.

5. Conclusions

- During early Eocene hyperthermals, Arctic landmasses were covered by broadleaf forests with the occurrence of palms and other subtropical elements. Bioclimatic analyses using nearest living relative analysis (NLR) and brGDGT paleothermometry indicate average mean annual temperatures during the PETM were ~2°-3.5 °C warmer, respectively, than the late Paleocene, reflecting the influence of winter warming of ~2.5 °C. Higher concentrations of massive AOM and dinocysts and dominance of low-salinity dinocysts are indicative of greater river runoff and increased flux of nutrients from the continent into the ocean. These changes caused greater stratification of the water column, algal blooms, and hypoxic conditions during hyperthermals.
- During the transition out of the PETM, needle-leaved forested

wetlands dominated Arctic landscapes, and mean annual temperatures remained warmer than during the late Paleocene. Dominance of granular AOM (palynofacies) and normal marine dinocysts indicate a reduced stratification of the water column related to decreased precipitation and inflow from the continents.

Supplementary data to this article can be found online at https://doi.org/10.1016/j.gloplacha.2019.04.012.

Acknowledgements

This work used samples and data provided by the International Ocean Discovery Program. DAW gratefully acknowledges support from the US Geological Survey Climate Research & Development Program. DRG's contribution was funded by a grant from the Natural Sciences and Engineering Research Council of Canada. The European Research Council under the European Community's Seventh Framework Program provided funding for this work by ERC Starting Grant #259627 to AS. SS and AS thank the Netherlands Organisation for Scientific Research for Gravitation Grant. We thank co-chiefs Jan Backman and Kate Moran and the Expedition 302 Scientists for providing the basis for this study, and Jan van Tongeren, Natasja Welters for technical support. We appreciate thoughtful comments from Tom Cronin, Steve Jackson, Robert Spicer, Torsten Utescher, and Lynn Wingard on earlier versions of the manuscript.

Data availability

The complete dataset of raw pollen/spore and palynofacies counts, brGDGT reconstructions of MAT, and bioclimatic estimates and underlying data are available online at the NOAA National Centers for Environmental Information (https://www.ncdc.noaa.gov/paleo/study/26590).

References

Backman, J., Moran, K., McInroy, D.B., Mayer, L.A., Expedition 302 Scientists, 2006. Expedition 302 Summary. Proc. IODP 302https://doi.org/10.2204/iodp.proc.302.2006. Edinburgh (Integrated Ocean Drilling Program Management International, Inc.).

Batten, D.J., 1983. Identification of amorphous sedimentary organic matter by transmitted light microscopy. Geol. Soc. Lond. Spec. Publ. 12, 275–287. https://doi.org/10.1144/GSL.SP.1983.012.01.28.

Batten, D.J., 1996. Palynofacies and paleoenvironmental interpretation. In: Palynology: Principles and Applications, American Association of Stratigraphic Palynologists Foundation, pp. 1011–1064.

Blach-Overgaard, A., Svenning, J.-C., Dransfield, J., Greve, M., Balslev, H., 2010. Determinants of palm species distributions across Africa: the relative roles of climate, non-climatic environmental factors, and spatial constraints. Ecography 33, 380–391. https://doi.org/10.1111/j.1600-0587.2010.06273.x.

Boulter, M.C., Manum, S.B., 1989. The Brito-Arctic igneous province flora around the Paleocene/Eocene boundary. Proc. Ocean Drill. Program Sci. Results 104, 663–680.

Buckles, L.K., Verschuren, D., Weijers, J.W.H., Cocquyt, C., Blaauw, M., Sinninghe Damsté, J.S., 2016. Interannual and (multi-)decadal variability in the sedimentary BIT index of Lake Challa, East Africa, over the past 2200 years: assessment of the precipitation proxy. Clim. Past 12, 1243–1262. https://doi.org/10.5194/cp-12-1243-2016.

Collinson, M.E., Steart, D.C., Harrington, G.J., Hooker, J.J., Scott, A.C., Allen, L.O., Glasspool, I.J., Gibbons, S.J., 2009. Palynological evidence of vegetation dynamics in response to palaeoenvironmental change across the onset of the Paleocene-Eocene Thermal Maximum at Cobham, Southern England. Grana 48, 38–66. https://doi.org/10.1080/00173130802707980.

Daly, R.J., Jolley, D.W., Spicer, R.A., 2011. The role of angiosperms in Palaeocene arctic ecosystems: a palynological study from the Alaskan North Slope. Palaeogeogr. Palaeoclimatol. Palaeoecol. 309, 374–382. https://doi.org/10.1016/j.palaeo.2011.07.007.

De Jonge, C., Hopmans, E.C., Zell, C.I., Kim, J.-H., Schouten, S., Sinninghe Damsté, J.S., 2014. Occurrence and abundance of 6-methyl branched glycerol dialkyl glycerol tetraethers in soils: implications for palaeoclimate reconstruction. Geochim. Cosmochim. Acta 141, 97–112. https://doi.org/10.1016/j.gca.2014.06.013.

Dransfield, J., Uhl, N.W., Asmussen, C.B., Baker, W.J., Harley, M.M., Lewis, C.E., 2008. Genera Palmarum: The Evolution and Classification of Palms. Kew Publishing, Kew.

Dunkley Jones, T., Lunt, D.J., Schmidt, D.N., Ridgwell, A., Sluijs, A., Valdes, P.J., Maslin, M., 2013. Climate model and proxy data constraints on ocean warming across the Paleocene–Eocene Thermal Maximum. Earth-Sci. Rev. 125, 123–145. https://doi.org/10.1016/j.earscirev.2013.07.004.

Eberle, J.J., Greenwood, D.R., 2012. Life at the top of the greenhouse Eocene world – a review of the Eocene flora and vertebrate fauna from Canada's High Arctic. Geol. Soc. Am. Bull. 124, 3–23. https://doi.org/10.1130/B30571.1.

Eldrett, J.S., Greenwood, D.R., Polling, M., Brinkhuis, H., Sluijs, A., 2014. A seasonality trigger for carbon injection at the Paleocene–Eocene Thermal Maximum. Clim. Past 10, 759–769.

Ercegovac, M., Kostić, A., 2006. Organic facies and palynofacies: nomenclature, classification and applicability for petroleum source rock evaluation. Int. J. Coal Geol. 68, 70–78. https://doi.org/10.1016/j.coal.2005.11.009.

GBIF.org, 2018. 27 June. GBIF Occurrence Download. https://doi.org/10.15468/dl.j6ob9o.

Greenwood, D.R., Basinger, J.F., 1994. The paleoecology of high-latitude Eocene swamp forests from Axel Heiberg Island, Canadian High Arctic. Rev. Palaeobot. Palynol. 81, 83–97. https://doi.org/10.1016/0034-6667(94)90128-7.

Greenwood, D.R., Wing, S.L., 1995. Eocene continental climates and latitudinal temperature gradients. Geology 23, 1044–1048. https://doi.org/10.1130/0091-7613(1995)023<1044:ECCALT>2.3.CO;2.

Greenwood, D.R., West, C.K., 2017. A fossil coryphoid palm from the Paleocene of western Canada. Rev. Palaeobot. Palynol. 239, 55–65.

Greenwood, D.R., Moss, P.T., Rowett, A.I., Vadala, A.J., Keefe, R.L., 2003. Plant communities and climate change in southeastern Australia during the early Paleogene. In: Causes and Consequences of Globally Warm Climates in the Early Paleogene. vol. 369. pp. 365–380. https://doi.org/10.1130/0-8137-2369-8.365. Geological Society of America Special Paper.

Greenwood, D.R., Archibald, S.B., Mathewes, R.W., Moss, P.T., 2005. Fossil biotas from the Okanagan Highlands, southern British Columbia and northeastern Washington State: climates and ecosystems across an Eocene landscape. Can. J. Earth Sci. 42, 167–185. https://doi.org/10.1139/e04-100.

Greenwood, D.R., Basinger, J.F., Smith, R.Y., 2010. How wet was the Arctic Eocene rain forest? Estimates of precipitation from Paleogene Arctic macrofloras. Geology 38, 15–18. https://doi.org/10.1130/G30218.1.

Greenwood, D.R., Keefe, R.L., Reichgelt, T., Webb, J.A., 2017. Eocene paleobotanical altimetry of Victoria's Eastern Uplands. Aust. J. Earth Sci. 64, 625–637. https://doi.org/10.1080/08120099.2017.1318793.

Grimm, G.W., Potts, A.J., 2016. Fallacies and fantasies: the theoretical underpinnings of the Coexistence Approach for palaeoclimate reconstruction. Clim. Past 12, 611–622. https://doi.org/10.5194/cp-12-611-2016.

Harbert, R.S., Nixon, K.C., 2015. Climate reconstruction analysis using coexistence likelihood estimation (CRACLE): a method for the estimation of climate using vegetation. Am. J. Bot. 102, 1277–1289. https://doi.org/10.3732/ajb.1400500.

Harding, I.C., Charles, A.J., Marshall, J.E.A., Pälike, H., Roberts, A.P., Wilson, P.A., Jarvis, E., Thorne, R., Morris, E., Moremon, R., Pearce, R.B., Akbari, S., 2011. Sea-level and salinity fluctuations during the Paleocene–Eocene thermal maximum in Arctic Spitsbergen. Earth Planet. Sci. Lett. 303, 97–107. https://doi.org/10.1016/j.epsl.2010.12.043.

Hart, G.F., 1986. Origin and classification of organic matter in clastic systems. Palynology (1), 1–23.

Hijmans, R.J., Cameron, S.E., Parra, J.L., Jones, P.G., Jarvis, A., 2005. Very high resolution interpolated climate surfaces for global land areas. Int. J. Climatol. 25, 1965–1978. https://doi.org/10.1002/joc.1276.

Hooghiemstra, H., 1988. Palynological record from northwest African marine sediments: a general outline of the interpretation of the pollen signal. Philos. Trans. R. Soc. B 318, 431–449.

Hopmans, E.C., Schouten, S., Sinningeh Damsté, J.S., 2016. The effect of improved chromatography on GDGT-based palaeoproxies. Organic Geochemistry 93, 1–6. https://doi.org/10.1016/j.orggeochem.2015.12.006.

Hyland, E.G., Huntington, K.W., Sheldon, N.D., Reichgelt, T., 2018. Temperature seasonality in the North American continental interior during the early Eocene climatic optimum. Clim. Past Discuss. 1–39. https://doi.org/10.5194/cp-2018-28.

Jackson, S.T., Lyford, M.E., 1999. Pollen dispersal models in quaternary plant ecology: assumptions, parameters, and prescriptions. Bot. Rev. 65, 39–75.

Jolley, D.W., Morton, A.C., 2007. Understanding basin sedimentary provenance: evidence from allied phytogeographic and heavy mineral analysis of the Palaeocene of the NE Atlantic. J. Geol. Soc. 164, 553–563. https://doi.org/10.1144/0016-76492005-187.

Jolley, D.W., Whitham, A.G., 2004. A stratigraphical and palaeoenvironmental analysis of the sub-basaltic Palaeogene sediments of East Greenland. Pet. Geosci. 10, 53–60. https://doi.org/10.1144/1354-079302-511.

Jolley, D.W., Bell, B.R., Williamson, I.T., Prince, I., 2009. Syn-eruption vegetation dynamics, paleosurfaces and structural controls on lava field vegetation: an example from the Palaeogene Staffa Formation, Mull Lava Field, Scotland. Rev. Palaeobot. Palynol. 153, 19–33. https://doi.org/10.1016/j.revpalbo.2008.06.003.

Kender, S., Stephenson, M.H., Riding, J.B., Leng, M.J., Knox, R.W.O., Peck, V.L., Kendrick, C.P., Ellis, M.A., Vane, C.H., Jamieson, R., 2012. Marine and terrestrial environmental changes in NW Europe preceding carbon release at the Paleocene–Eocene transition. Earth Planet. Sci. Lett. 353–354, 108–120. https://doi.org/10.1016/j.epsl.2012.08.011.

Lourens, L.J., Sluijs, A., Kroon, D., Zachos, J.C., Thomas, E., Röhl, U., Bowles, J., Raffi, I., 2005. Astronomical pacing of late Palaeocene to early Eocene global warming events. Nature 435, 1083–1087. https://doi.org/10.1038/nature03814.

Martinez, N.C., Murray, R.W., Dickens, G.R., Kölling, M., 2009. Discrimination of sources of terrigenous sediment deposited in the central Arctic Ocean through the Cenozoic: Terrigenous sources of the Arctic Ocean. Paleoceanography 24. https://doi.org/10.1029/2007PA001567.

Masson-Delmotte, V., 2013. Information from Paleoclimate Archives. In: Climate Change 2013: The Physical Science Basis. Contribution of Working Group I to the Fifth

Assessment Report of the Intergovernmental Panel on Climate Change. Cambridge University Press, Cambridge, United Kingdom and New York, NY.
McNeil, D.H., Parsons, M.G., 2013. The Paleocene-Eocene thermal maximum in the Arctic Beaufort-Mackenzie Basin – Palynomorphs, carbon isotopes and benthic foraminiferal turnover. Bull. Can. Petrol. Geol. 61, 157–186. https://doi.org/10.2113/gscpgbull.61.2.157.
Moran, K., Backman, J., Brinkhuis, H., Clemens, S.C., Cronin, T., Dickens, G.R., Eynaud, F., Gattacceca, J., Jakobsson, M., Jordan, R.W., Kaminski, M., King, J., Koc, N., Krylov, A., Martinez, N., Matthiessen, J., McInroy, D., Moore, T.C., Onodera, J., O'Regan, M., Pälike, H., Rea, B., Rio, D., Sakamoto, T., Smith, D.C., Stein, R., St John, K., Suto, I., Suzuki, N., Takahashi, K., Watanabe, M., Yamamoto, M., Farrell, J., Frank, M., Kubik, P., Jokat, W., Kristoffersen, Y., 2006. The Cenozoic palaeoenvironment of the Arctic Ocean. Nature 441, 601–605. https://doi.org/10.1038/nature04800.
Mosbrugger, V., Gee, C.T., Belz, G., Ashraf, A.R., 1994. Three-dimensional reconstruction of an in-situ Miocene peat forest from the lower Rhine Embayment, northwestern Germany – new methods in palaeovegetation analysis. Palaeogeogr. Palaeoclimatol. Palaeoecol. 110, 295–317.
Mudie, P.J., McCarthy, F.M.G., 1994. Late Quaternary pollen transport processes, western North Atlantic: data from box models, cross-margin and N-S transects. Mar. Geol. 118, 79–105. https://doi.org/10.1016/0025-3227(94)90114-7.
Mudie, P.J., McCarthy, F.M.G., 2006. Marine palynology: potentials for onshore – offshore correlation of Pleistocene—Holocene records. Trans. R. Soc. S. Afr. 61, 139–157. https://doi.org/10.1080/00359190609519964.
Pacton, M., Gorin, G.E., Vasconcelos, C., 2011. Amorphous organic matter – experimental data on formation and the role of microbes. Rev. Palaeobot. Palynol. 166, 253–267. https://doi.org/10.1016/j.revpalbo.2011.05.011.
Pagani, M., Pedentchouk, N., Huber, M., Sluijs, A., Schouten, S., Brinkhuis, H., Sinninghe Damsté, J.S., Dickens, G.R., 2006. Arctic hydrology during global warming at the Palaeocene/Eocene thermal maximum. Nature 442, 671–675. https://doi.org/10.1038/nature05043.
Panchuk, K., Ridgwell, A., Kump, L.R., 2008. Sedimentary response to Paleocene-Eocene Thermal Maximum carbon release: a model-data comparison. Geology 36, 315. https://doi.org/10.1130/G24474A.1.
Peterse, F., Kim, J.H., Schouten, S., Kristensen, D.K., Koç, N., Sinninghe Damsté, J.S., 2009. Constraints on the application of the MBT/CBT palaeothermometer at high latitude environments (Svalbard, Norway). Org. Geochem. 40, 692–699.
Pierrehumbert, R.T., 2002. The hydrologic cycle in deep-time climate problems. Nature 419, 191–198. https://doi.org/10.1038/nature01088.
Pross, J., Contreras, L., Bijl, P.K., Greenwood, D.R., Bohaty, S.M., Schouten, S., Bendle, J.A., Röhl, U., Tauxe, L., Raine, J.I., Huck, C.E., van de Flierdt, T., Jamieson, S.S.R., Stickley, C.E., van de Schootbrugge, B., Escutia, C., Brinkhuis, H., 2012. Persistent near-tropical warmth on the Antarctic continent during the early Eocene epoch. Nature 488, 73–77. https://doi.org/10.1038/nature11300.
Reichgelt, T., Kennedy, E.M., Jones, W.A., Jones, D.T., Lee, D.E., 2016. Contrasting palaeoenvironments of the mid/late Miocene Dunedin Volcano, southern New Zealand: climate or topography? Palaeogeogr. Palaeoclimatol. Palaeoecol. 441, 696–703.
Reichgelt, T., West, C.K., Greenwood, D.R., 2018. The relation between global palm distribution and climate. Sci. Rep. 8. https://doi.org/10.1038/s41598-018-23147-2.
Schweitzer, H.-J., 1980. Environment and climate in the early Tertiary of Spitsbergen. Palaeogeogr. Palaeoclimatol. Palaeoecol. 30, 297–311. https://doi.org/10.1016/0031-0182(80)90062-0.
Self-Trail, J.M., Robinson, M.M., Bralower, T.J., Sessa, J.A., Hajek, E.A., Kump, L.R., Trampush, S.M., Willard, D.A., Edwards, L.E., Powars, D.S., Wandless, G.A., 2017. Shallow marine response to global climate change during the Paleocene-Eocene Thermal Maximum, Salisbury Embayment, USA: PETM Coastal Response. Paleoceanography 32, 710–728. https://doi.org/10.1002/2017PA003096.
Sinninghe Damsté, J.S., 2016. Spatial heterogeneity of sources of branched tetraethers in shelf systems: the geochemistry of tetraethers in the Berau River delta (Kalimantan, Indonesia). Geochim. Cosmochim. Acta 186, 13–31. https://doi.org/10.1016/j.gca.2016.04.033.
Sluijs, A., Brinkhuis, H., Crouch, E.M., John, C.M., Handley, L., Munsterman, D., Bohaty, S.M., Zachos, J.C., Reichart, G.-J., Schouten, S., Pancost, R.D., Sinninghe Damsté, J.S., Welters, N.L.D., Lotter, A.F., Dickens, G.R., 2008. Eustatic variations during the Paleocene-Eocene greenhouse world. Paleoceanography 23, PA4216. https://doi.org/10.1029/2008PA001615.
Sluijs, A., Dickens, G.R., 2012. Assessing offsets between the δ^{13}C of sedimentary components and the global exogenic carbon pool across early Paleogene carbon cycle perturbations. Glob. Biogeochem. Cycles 26. https://doi.org/10.1029/2011GB004224.
Sluijs, A., Schouten, S., Pagani, M., Woltering, M., Brinkhuis, H., Damsté, J.S.S., Dickens, G.R., Huber, M., Reichart, G.-J., Stein, R., Matthiessen, J., Lourens, L.J., Pedentchouk, N., Backman, J., Moran, K., 2006. Subtropical Arctic Ocean temperatures during the Palaeocene/Eocene thermal maximum. Nature 441, 610–613. https://doi.org/10.1038/nature04668.
Sluijs, A., Schouten, S., Donders, T.H., Schoon, P.L., Röhl, U., Reichart, G.-J., Sangiorgi, F., Kim, J.-H., Sinninghe Damsté, J.S., Brinkhuis, H., 2009. Warm and wet conditions in the Arctic region during Eocene Thermal Maximum 2. Nat. Geosci. 2, 777–780. https://doi.org/10.1038/ngeo668.
Smith, F., Wing, S., Freeman, K., 2007. Magnitude of the carbon isotope excursion at the Paleocene–Eocene thermal maximum: the role of plant community change. Earth Planet. Sci. Lett. 262, 50–65. https://doi.org/10.1016/j.epsl.2007.07.021.
Smith, R.W., Bianchi, T.S., Li, X., 2012. A re-evaluation of the use of branched GDGTs as terrestrial biomarkers: implications for the BIT index. Geochim. Cosmochim. Acta 80, 14–29.
Stap, L., Lourens, L., van Dijk, A., Schouten, S., Thomas, E., 2010a. Coherent pattern and timing of the carbon isotope excursion and warming during Eocene Thermal Maximum 2 as recorded in planktic and benthic foraminifera: planktic δ^{13}C and δ^{18}O records of ETM2. Geochem. Geophys. Geosyst. 11. https://doi.org/10.1029/2010GC003097.
Stap, L., Lourens, L.J., Thomas, E., Sluijs, A., Bohaty, S., Zachos, J.C., 2010b. High-resolution deep-sea carbon and oxygen isotope records of Eocene Thermal Maximum 2 and H2. Geology 38, 607–610. https://doi.org/10.1130/G30777.1.
Stockmarr, J., 1971. Tablets with spores used in absolute pollen analysis. Pollen Spores 13, 615–622.
Suan, G., Popescu, S.-M., Suc, J.-P., Schnyder, J., Fauquette, S., Baudin, F., Yoon, D., Piepjohn, K., Sobolev, N.N., Labrousse, L., 2017. Subtropical climate conditions and mangrove growth in Arctic Siberia during the early Eocene. Geology 45, 539–542. https://doi.org/10.1130/G38547.1.
Thompson, R.S., Anderson, K.H., Pelltier, R.T., Strickland, L.E., Bartlein, P.J., Shafer, S.L., 2012. Quantitative estimation of climatic parameters from vegetation data in North America by the mutual climatic range technique. Quat. Sci. Rev. 51, 18–39. https://doi.org/10.1016/j.quascirev.2012.07.003.
Trujillo, A.P., 2009. Paleocene-Eocene Palynology and Palynofacies from Northeastern Colombia and Western Venezuela. Centro Editorial Universidad De Caldas.
Tyson, R.V., 1993. Palynofacies analysis. In: Applied Micropalaeontology. Springer, Dordrecht, pp. 153–191.
Utescher, T., Bruch, A.A., Erdei, B., François, L., Ivanov, D., Jacques, F.M.B., Kern, A.K., Liu, Y.-S.C., Mosbrugger, V., Spicer, R.A., 2014. The Coexistence Approach—theoretical background and practical considerations of using plant fossils for climate quantification. Palaeogeogr. Palaeoclimatol. Palaeoecol. 410, 58–73. https://doi.org/10.1016/j.palaeo.2014.05.031.
Walther, G.-R., Gritti, E.S., Berger, S., Hickler, T., Tang, Z., Sykes, M.T., 2007. Palms tracking climate change. Glob. Ecol. Biogeogr. 16, 801–809. https://doi.org/10.1111/j.1466-8238.2007.00328.x.
Weijers, J.W.H., Schouten, S., van den Donker, J.C., Hopmans, E.C., Sinninghe Damsté, J.S., 2007a. Environmental controls on bacterial tetraether membrane lipid distribution in soils. Geochim. Cosmochim. Acta 71, 703–713. https://doi.org/10.1016/j.gca.2006.10.003.
Weijers, J.W.H., Schefuss, E., Schouten, S., Sinninghe Damsté, J.S., 2007b. Coupled thermal and hydrological evolution of tropical Africa over the last deglaciation. Science 315, 1701–1704. https://doi.org/10.1126/science.1138131.
West, C.K., Greenwood, D.R., Basinger, J.F., 2015. Was the Arctic Eocene 'rainforest' monsoonal? Estimates of seasonal precipitation from early Eocene megafloras from Ellesmere Island, Nunavut. Earth Planet. Sci. Lett. 427, 18–30. https://doi.org/10.1016/j.epsl.2015.06.036.
Wing, S.L., 2005. Transient floral change and rapid global warming at the Paleocene-Eocene boundary. Science 310, 993–996. https://doi.org/10.1126/science.1116913.
Wing, S.L., Currano, E.D., 2013. Plant response to a global greenhouse event 56 million years ago. Am. J. Bot. 100, 1234–1254. https://doi.org/10.3732/ajb.1200554.
Wolfe, J.A., 1979. Temperature parameters of humid to mesic forests of eastern Asia and relation to forests of other regions of the Northern Hemisphere and Australasia. U.S. Geological Survey Professional Paper 1106, 1–37. https://pubs.er.usgs.gov/publication/pp1106.
Wood, S.E., Gorin, G.E., 1998. Sedimentary organic matter in distal clinoforms of Miocene slope sediments: site 903 of ODP Leg 150, offshore New Jersey (U.S.A.). J. Sediment. Res. 68, 856–878. https://doi.org/10.2110/jsr.68.856.
Zachos, J.C., 2005. Rapid acidification of the Ocean during the Paleocene-Eocene Thermal Maximum. Science 308, 1611–1615. https://doi.org/10.1126/science.1109004.
Zeebe, R.E., Zachos, J.C., Dickens, G.R., 2009. Carbon dioxide forcing alone insufficient to explain Palaeocene–Eocene Thermal Maximum warming. Nat. Geosci. 2, 576–580. https://doi.org/10.1038/ngeo578.